Corrected 28 September 2020. See full text.

RESEARCH ARTICLE

NITROGEN FIXATION

A bound reaction intermediate sheds light on the mechanism of nitrogenase

Daniel Sippel,[1] Michael Rohde,[1] Julia Netzer,[1] Christian Trncik,[1] Jakob Gies,[1] Katharina Grunau,[1] Ivana Djurdjevic,[1] Laure Decamps,[1] Susana L. A. Andrade,[1,2] Oliver Einsle[1,2,3]*

Reduction of N_2 by nitrogenases occurs at an organometallic iron cofactor that commonly also contains either molybdenum or vanadium. The well-characterized resting state of the cofactor does not bind substrate, so its mode of action remains enigmatic. Carbon monoxide was recently found to replace a bridging sulfide, but the mechanistic relevance was unclear. Here we report the structural analysis of vanadium nitrogenase with a bound intermediate, interpreted as a μ^2-bridging, protonated nitrogen that implies the site and mode of substrate binding to the cofactor. Binding results in a flip of amino acid glutamine 176, which hydrogen-bonds the ligand and creates a holding position for the displaced sulfide. The intermediate likely represents state E_6 or E_7 of the Thorneley-Lowe model and provides clues to the remainder of the catalytic cycle.

Nitrogen bioavailability is limited by the chemical stability of N_2 gas, making modern agriculture dependent on inorganic nitrogen fertilizers that have boosted crop yields during the 20th century to enable unprecedented population growth (*1*). Today, excessive fertilization is leading to increasing environmental release of reactive nitrogen species that affect water quality and human health (*2*). Alternative strategies for sustained crop production are sought, and among these, the enzyme nitrogenase—the sole biological solution for reducing atmospheric N_2—is of outstanding importance. It provides fixed nitrogen in the exact quantities required and operates at ambient conditions, fueled by adenosine triphosphate (ATP) (*3*, *4*). Nitrogenase is an oxygen-sensitive metalloenzyme consisting of a reductase, Fe protein, and a catalytic dinitrogenase that dynamically form a complex for every single-electron transfer event, triggered by ATP hydrolysis in Fe protein (*4*–*6*). All nitrogenases share a single evolutionary origin, but they group into three different classes according to the metal ions used at the catalytic site (*7*). In the most widespread molybdenum nitrogenases, this site is FeMo cofactor, a [Mo:7Fe:9S:C]:homocitrate cluster with a central carbide for structural rigidity (*6*, *8*), an apical Mo^{3+} (*9*), and three characteristic "belt" sulfides termed S2B, S3A, and S5A (fig. S1A) (*10*). Alternative nitrogenases are produced from distinct gene clusters under molybdenum limitation and replace molybdenum with vanadium (FeV cofactor) or iron (FeFe cofactor). FeV cofactor, a [V:7Fe:8S:C]:CO_3:homocitrate moiety in VFe protein, resembles FeMo cofactor but features a carbonate replacing S3A (fig. S1B) (*11*). Mo and V nitrogenases differ in potential and reactivity (*12*), most notably in that the MoFe protein inhibitor carbon monoxide (CO) is reduced by VFe protein to various hydrocarbons, in analogy to Fischer-Tropsch chemistry (*13*).

Before this work, all nitrogenases were isolated in a stable resting state, and because reduction requires the dynamic action of Fe protein, structural analysis to date was largely limited to this form. Mechanistic studies pioneered by Bulen and Lecomte showed H_2 to be a by-product of N_2 reduction (*14*), and Simpson and Burris found that it occurs at least stoichiometrically (*15*), leading Thorneley and Lowe (*16*) to outline an eight-electron catalytic cycle (states E_0 to E_7) for the six-electron reduction of N_2 and the concomitant generation of H_2. In the Thorneley-Lowe model, reduction of the enzyme by three or four electrons is required before N_2 binds in exchange for H_2 (fig. S2) (*16*, *17*), whereby N_2 is the only substrate whose reduction is inhibited by H_2 (*18*). The question of how an already highly reduced cofactor accumulates three or four more electrons at isopotential was addressed by studying ligand binding to variants of MoFe protein, which suggested that electrons are stored as hydrides (H^-) on the cluster surface (*19*, *20*), in line with earlier findings that at no point would the cluster itself take up more than a single electron (*21*). In the critical E_4 state, two adjacent hydrides would undergo reductive elimination of H_2, leaving the metal site reduced by two low-potential electrons that render it capable of binding and activating N_2 (*22*, *23*). Based on a $V70^{NifD}$ variant, Fe6 and the cluster face located beneath V70 and framed by Fe2, Fe3, Fe6, and Fe7 were indirectly implied as the site of N_2 binding (*24*). From this point, a deeper mechanistic understanding of nitrogenase catalysis thus awaits the assignment of actual molecular structures to reaction intermediates E_1 through E_7. When CO inhibition of Mo dinitrogenase was recently exploited to obtain the first ligand-bound structure of FeMo cofactor (*25*), CO replaced belt sulfide S2B, yielding a μ^2-bridging metal carbonyl (fig. S1C). However, CO is a noncompetitive inhibitor that binds to a less reduced form of the enzyme than N_2 does, presumably E_2 (*26*), and it was unclear how the observed binding mode related to N_2 catalysis. Importantly, although sulfide S2B was quantitatively replaced and was not detected in the immediate vicinity of the cofactor in the inhibited state, the subsequent removal of CO under turnover was sufficient to reinstate S2B and return the enzyme to the known resting state (*25*). The structure of VFe protein showed the E_0 state, with carbonate replacing sulfide S3A, whereas S2B remained unchanged (*11*). All of the different nitrogenases presumably share a common mechanism of dinitrogen activation and reduction. For further mechanistic insight, we thus set out to elucidate a nonresting state of the enzyme by x-ray crystallography.

Generation of a ligand-binding site on the cofactor

Previously, induction of VFe protein by Mo depletion and isolation in the presence of 2 to 5 mM $Na_2S_2O_4$ (*11*), serving as a reductant and O_2 scavenger, yielded pure enzyme and led to a structure at 1.35 Å of the resting state of FeV cofactor (*11*). We subsequently noted that if the isolation process was carried out swiftly and with a decreased amount of reductant, the intensity of electron paramagnetic resonance (EPR) signals—but not their position—changed characteristically (Fig. 1B). This gradual transition varied between preparations, but prolonged reduction with 20 mM dithionite consistently resulted in resting state spectra. Notably, both forms of the enzyme retained the same catalytic activity and reduced both acetylene and N_2 (fig. S3). Accordingly, decreasing the amount of reductant during protein isolation led to well-diffracting crystals of an uncharacterized state of V nitrogenase that we designate the "turnover" state. Several data sets were obtained to investigate the anomalous contributions of Fe and S, and diffraction data were collected at 1.2-Å resolution (fig. S4). VFe protein remained largely unchanged, including in particular the carbonate ligand bridging Fe4 and Fe5 of FeV cofactor, but the cluster contained a light atom replacing sulfide S2B.

The lability of the belt sulfides was established by the CO-inhibited structure of MoFe protein, but the fate of the released S2B remained unclear, and an anomalous difference density peak found at a distance of 21 Å from the cofactor was difficult to reconcile with an integral mechanistic

[1]Institut für Biochemie, Albert-Ludwigs-Universität Freiburg, Albertstraße 21, 79104 Freiburg, Germany. [2]BIOSS Centre for Biological Signalling Studies, Schänzlestraße 1, 79104 Freiburg, Germany. [3]Freiburg Institute for Advanced Studies, 79104 Freiburg, Germany.
*Corresponding author. Email: einsle@biochemie.uni-freiburg.de

Corrected 28 September 2020. See full text.

role of the sulfide exchange (*25*). Unfortunately, no structural data are available for the variants of Mo nitrogenase used for the cryo-annealing pulsed EPR studies that defined activated states (*27*). The ligand-bound form of VFe protein reported here provides a picture of a nitrogenase in a nonresting state obtained during N_2 turnover, with a previously uncharacterized μ^2-bridging ligand to Fe2 and Fe6 displacing S2B (Figs. 1A and 2A). In contrast to the CO complex of FeMo cofactor (*25*), the displacement in VFe protein rearranged a nearby amino acid, glutamine 176 (Q176), which is conserved in all known structures of nitrogenases (Q191 in *Azotobacter vinelandii* MoFe protein; fig. S5). Its replacement by lysine abolished N_2 reduction and strongly diverted electron flux away from C_2H_2 toward H_2 (*28*, *29*), but given that it pointed away from the cofactor, a role in catalysis remained unclear (fig. S5, C to H). In the turnover state, the side chain of Q176 rotated toward the FeV cofactor, placing the amide oxygen atom Oε1 at a distance of only 2.55 Å from the bridging light atom and 2.84 Å from imidazole Nε2 of residue histidine 180 (H180) (Fig. 2A), while retaining an H-bonding interaction with the α-carboxylate of homocitrate. The tight fixation of Oε1 of Q176 by three short hydrogen bonds would not be possible with a diatomic ligand at the cofactor, and glutamine rotation did not occur in the CO complex structure, where the carbonyl oxygen of the ligand is an exclusive H-bond acceptor (fig. S6) (*25*). It could also not be accommodated with S2B bridging Fe2 and Fe6 in the resting state of the enzyme, because the longer Fe–S distances of 2.3 Å compared with the distance to the light atom bound at 2.0 Å would leave no room for an inward-facing Q176 to form a direct hydrogen bond to H180 (Fig. 2B and fig. S7, A and B). Furthermore, the glutamine reorientation created a binding pocket within the protein cavity containing the cofactor, where we observed a new electron density maximum that was well modeled as a hydrosulfide anion (HS^-) (Fig. 1A). This makes the site a strong candidate for the long-sought temporary holding position for sulfide S2B close to the cofactor, which the CO complex did not reveal. To confirm the presence of HS^-, we collected diffraction data on the resting and ligand-bound states of VFe protein at 7000 eV (wavelength, 1.7711 Å) to maximize the anomalous scattering contribution of sulfur with respect to that of iron (Fig. 2, C and D). The resulting electron density maps show the disappearance of the anomalous signal at the bridging position in the cofactor and its reappearance 7.0 Å away, in the pocket created by the rotation of Q176 (Fig. 2C), whereas in the resting state, S2B was in place at the cofactor (Fig. 2D). In its holding position, S2B is H-bonded to the backbone amides of glycine 48 (3.13 Å) and Q176 (3.13 Å) that transiently stabilize its negative charge (Fig. 2A), reminiscent of an oxyanion hole in protease active sites (*30*).

We conclude that replacement of S2B at the cofactor is reversible and can occur during catalysis, with intermediate storage in a pocket provided by the side-chain swing of Q176, whose amide Oε1 interacts with the same residues in the resting state as HS^- does in the turnover state (Fig. 2, A and B). This defines an open active site at nitrogenase cofactor with free coordination sites for ligands at Fe2 and Fe6, residue H180 as a proton donor, and the inward-facing Oε1 of Q176 as an exclusive H-bond acceptor, marking its specific role in stabilizing protonated species. We assign the released sulfide as HS^-, given that rebinding at the conclusion of the reaction will be favored for a nucleophile.

Ligand binding to the active site

For our structure, cultures were harvested during diazotrophic growth, and neither cells nor isolated protein were exposed to CO, O_2, or further substrates other than N_2. At 1.2-Å resolution, we refrain from an assignment of the nature of the bridging ligand based solely on its electron density, but instead restrict our discussion to oxygen and nitrogen as chemically reasonable candidates. Bond distances at the cofactor were 2.01 ± 0.04 Å for the two Fe–X bonds and 2.55 Å for a short hydrogen bond to amide Oε1 of Q176. This implies a protonated ligand—either a μ-hydroxo (OH^-) or a μ-nitrido (HN^{2-}) species—in line with our electron density analysis (fig. S8 and supplementary materials) and as expected from diiron model compounds (*31*). These π-basic ligands would have a stabilizing effect, in particular with a more oxidized cluster, but are themselves fully reduced. μ-hydroxo represents the oxidation

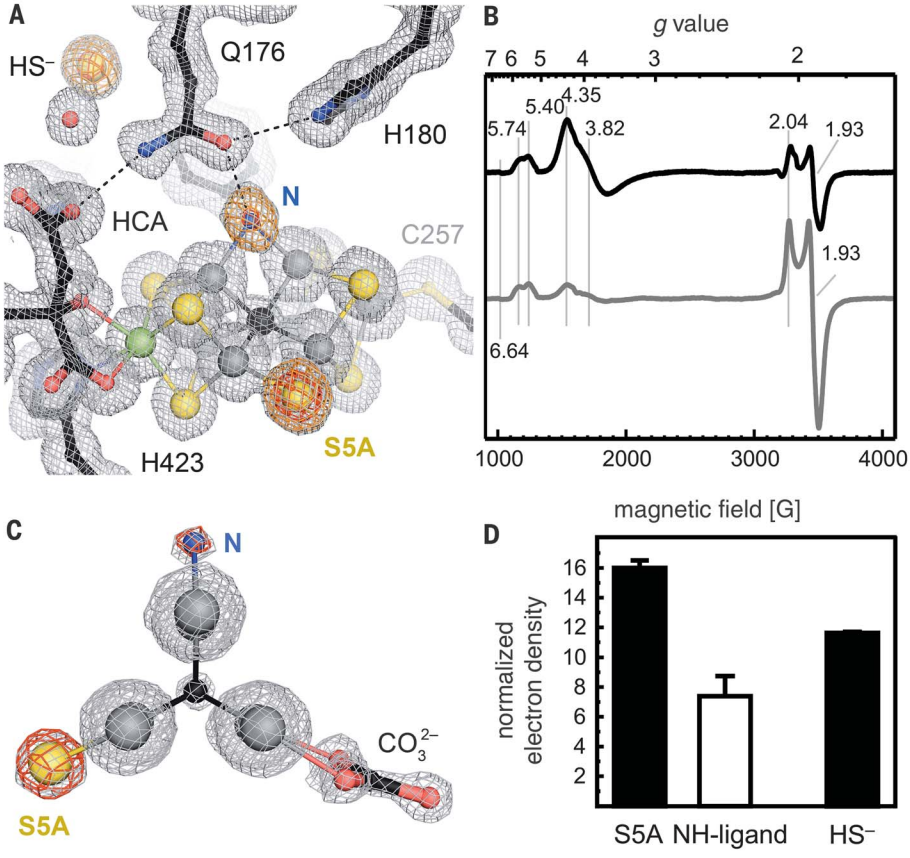

Fig. 1. Identification of a light atom ligand at FeV cofactor. (**A**) FeV cofactor and its immediate surroundings with residue Q176 in a flipped conformation, opening a binding site for sulfide S2B as HS^-. The bridging position of S2B at Fe2 and Fe6 is occupied by a light atom. A $2F_o–F_c$ omit electron density map calculated without the contribution of S2B, S5A, and the light atom is contoured at the 1σ level (gray) and is overlaid with $F_o–F_c$ omit maps contoured at 15σ (orange) and 25σ (red). C, cysteine. Here and throughout, spheres are color-coded as follows: gray, iron; black, carbon; green, vanadium; blue, nitrogen; yellow, sulfur. (**B**) X-band EPR spectra of *A. vinelandii* VFe protein as isolated in the turnover state (black) and the resting state (gray). The known features of the spectrum change their relative intensities, but not their resonance energies. (**C**) View along the threefold pseudo-symmetry axis of FeV cofactor, highlighting the differences at the three belt positions. The omit maps [as shown in (A)] highlight the differences between the light N ligand and sulfide S5A. The $2F_o–F_c$ map (gray) is contoured at the 10σ level. (**D**) Integrated electron density at the three omitted positions (1-Å integration radius, normalized to the electron number of the fully occupied S5A). The maximum at Fe2 and Fe6 is very well defined and matches an N or NH ligand.

Corrected 28 September 2020. See full text.

state of water and should be the more stable species. Although H_2O binding may be envisioned after the removal of S2B upon reduction to E_2 (discussed below), this would make water a competitive inhibitor of an enzymatic reaction, which would be biochemically peculiar, to say the least. O_2, as an alternative source of oxygen, can be ruled out owing to strictly anoxic handling of the enzyme and the proven activity of turnover state preparations. Similarly, a μ-nitrido ligand represents nitrogen at the oxidation level of ammonia (–III), the product after the completed eight-electron reaction cycle. This would be an E_0 state of the reaction scheme, albeit with bound product rather than with the μ-sulfide S2B reinstated, and may correspond to an "E_8" state previously reported as an interpretation of a spectroscopic intermediate "I" (*32*). In the case of our active preparations of VFe protein, this would imply that the reinsertion of sulfide was not an integral part of the reaction cycle under high electron flux. However, an HN^{2-} complex is only two protonation events removed from releasing NH_3, which should readily occur from H180, but we nevertheless find this state to be stable and persistent even on the time scale of protein crystallization. Together with the finding from EPR spectroscopy that turnover state preparations of VFe protein can be returned to the resting state by extended reduction (fig. S3B), this suggests that the observed structure is an earlier catalytic intermediate. Given that the state is paramagnetic (Fig. 2B), this should be E_6, at a formal oxidation state of –I for the bound nitrogen atom (Fig. 3, A and C), making the ligand formally a bridging nitrene. With its slightly distorted trigonal planar geometry (Fig. 3, A and B), this modification features an empty p_z-like orbital at the nitrogen atom that also stabilizes the intermediate, this time through π-backdonation from both iron sites and with strong preference for a more reduced form of the cofactor. Nitrenes are unstable compounds, but the proximity of Fe2 and Fe6 to the central carbon in the cofactor—formally a C^{4-}—may imply that the iron ions are effectively more reduced, or even that the cluster is able to transiently transfer two electrons to the ligand. Such a redox shift would result in a two-electron oxidized cluster (still with spin $S = 3/2$) and a stable HN^{2-} ligand as described above that nevertheless would represent state E_6 rather than the resting state E_0. Although speculative, this interpretation generates testable hypotheses for spectroscopic and theoretical studies that should unequivocally clarify the nature of the bound ligand.

From E_6, two single-electron reduction steps return the enzyme to the known resting state E_0, with S2B rebound and product NH_3 released. Assuming that the cluster itself is oxidized by two electrons at this stage, these reductions will take place on the cofactor, with each step successively decreasing the stabilizing effect of π-donation by the HN^{2-} ligand, rendering it prone to further protonation that will break the stabilizing, short hydrogen bond to Q176 to eventually release the bridging nitrogen in favor of end-on binding to either Fe2 or Fe6. We hypothesize that NH_2 will be bound at Fe2, as only there it can form a new short hydrogen bond to H180, with the imidazole Nε2 of this histidine as a possible proton donor (Fig. 3D). Q176 then loses both the ligand atom and H180 as H-bonding partners, whereas Fe6 gains a free coordination site for a nucleophilic attack by HS^-. This causes the glutamine to return to its resting position, concomitant with rebinding of the hydrogen sulfide ligand at Fe6. The final electron transfer to E_0 then enables the dissociation of NH_3, with the Fe6-SH group able to provide a proton to reform the μ^2 belt sulfide of the resting state E_0 (Fig. 3E). In this model, S2B is instrumental for product dissociation, in line with suggestions from theory (*33*).

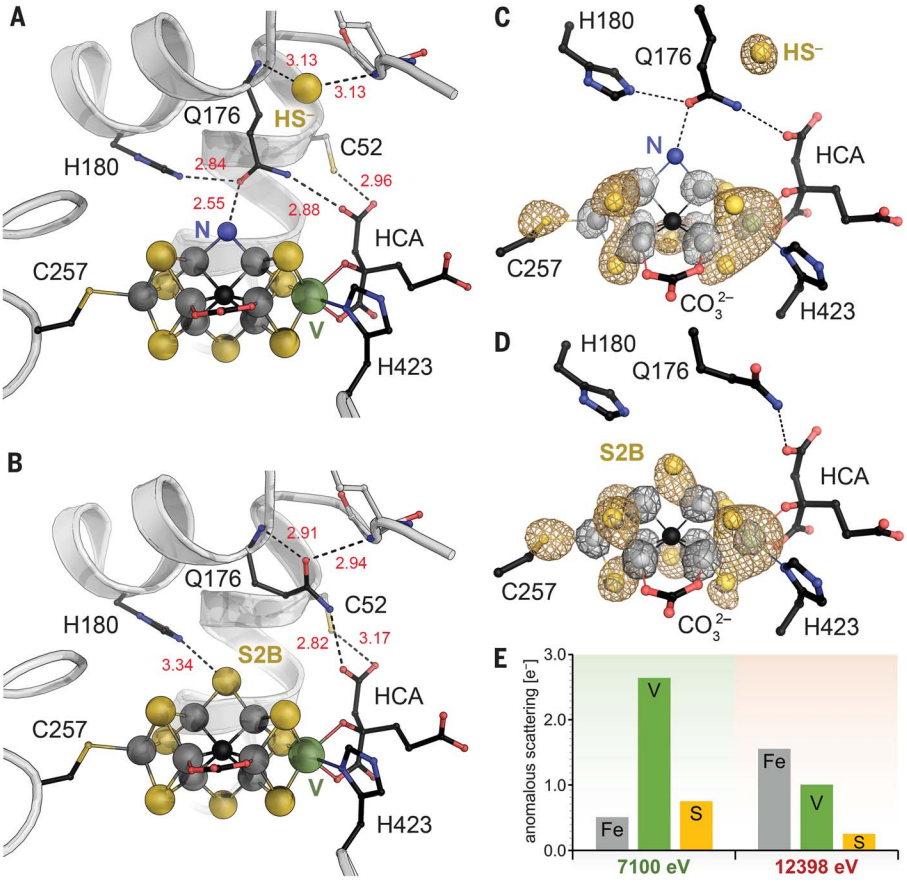

Fig. 2. Ligand-bound V nitrogenase in a turnover state. (**A**) FeV cofactor in the turnover state. Sulfide S2B is exchanged for a nitrogen ligand, and residue Q176 has rearranged, revealing a holding site for sulfide. (**B**) FeV cofactor in the resting state (Protein Data Bank ID, 5N6Y). S2B is in place, and Q176 occupies the holding site. Bond distances are in angstroms. (**C**) Turnover-state FeV cofactor, with anomalous difference electron density maps contoured at the 5σ level and collected at x-ray energies of 7000 eV (tan) for sulfur and 12398 eV (gray) for iron. The holding site shows a prominent peak for sulfur, whereas the bridging position at Fe2 and Fe6 does not. (**D**) In an analogous map for the resting-state enzyme, no electron density peak is observed in the holding site, but the bridging sulfide S2B is found at the cluster. (**E**) Relative anomalous scattering contributions of Fe, V, and S at the two energies used in (C) and (D). At 7100 eV, S shows a stronger signal than Fe, whereas at 12398 eV, the situation is the reverse. V is a strong contributor at both energies and the most dominant at 7100 eV.

Mechanistic axioms for nitrogenase catalysis

The structure of a nitrogenase turnover state establishes sulfide exchange in a bridging manner at Fe2 and Fe6 as part of the reaction mechanism and reveals the role of Q176 as an H-bond acceptor and a stabilizing structural element for intermediates of N_2 reduction. Although the power of x-ray diffraction to identify electronic states of individual atoms is limited, our structure has implications for earlier stages of the reaction cycle. Importantly, in spite of differences in activity and substrate range, all classes of nitrogenases are presumed to follow the same mechanistic pathway for N_2 reduction, and we therefore carefully extend data gained on MoFe protein to VFe protein. Also, the catalytic turnover of nitrogenase is rate-limited by electron delivery from Fe protein, which in turn is limited by the dissociation of phosphate (*34*). This implies that each E state must be sufficiently stable to persist until the

next electron transfer occurs. We thus avoid unfavorable geometries or unusual coordination numbers. Furthermore, bridging hydrides are thermodynamically more stable than terminal hydrides (*35*). Together with the demonstrated ability of nitrogenase cofactors to take up one electron only (*21*), the delivery of every second electron from Fe protein can give rise to a bridging hydride, and the reduction of substrate thus can be conceptually discussed in two-electron steps (*24*, *36*). At the same time, proton supply from the protein surface to the cluster is straightforward once H180 is recognized as the prime proton donor in catalysis (fig. S9), as much as Q176 is a stabilizing H-bond acceptor whose inward movement is reversibly linked to S2B displacement.

Implications for N_2 reduction by nitrogenase

During the entire catalytic cycle, the cofactor oscillates between only two redox states, paramagnetic M^N (as isolated) and diamagnetic M^{-1} (one-electron-reduced). According to the current model of the electronic structure of the cofactor (fig. S10) (*37*), Fe2 and Fe6 are the most oxidized sites and are antiferromagnetically coupled to their respective neighbors (except for the apical Fe1 and Mo or V). Initially, electron transfer from Fe protein reduces Fe2 or Fe6, defining state E_1. Further reduction to E_2 leads to the formation of a first hydride together with a proton. Bridging Fe2 and Fe6, this hydride should shift sulfide S2B out of the plane defined by Fe1, Fe2, Fe6, and Mo or V, as suggested previously (*33*). Alternatively, one or both Fe–S bonds to S2B may already be broken (Fig. 4A), in line with the presumed binding of CO at E_2 (*26*). An inward-facing Q176 might also stabilize a bridging hydride, but only after S2B moves to its holding site. If at this point the hydride is lost as H_2 owing to accidental protonation, an open, diferric binding site becomes available for CO but would not be sufficiently reduced for N_2. States E_2 through E_4 can lose H^- by protonation to yield H_2, rationalizing the observed nonproductive electron flux to this shunt product (fig. S2).

N_2 binding to cofactor occurs no earlier than at E_3, where the association is reversible until further reduction, or at E_4, from which the reaction is committed to proceed to ammonia release (*38*). We propose that E_3 retains the structural features of E_2, but with one Fe site reduced to formal Fe^{2+}, rendering the state diamagnetic. From this, H_2 release would leave the cluster in a one-electron-reduced state with S2B removed and able to bind N_2, but without constituting a reductive elimination and lacking a further electron for a bridging binding mode (Fig. 4A). This binding is reversible, with N_2 as a leaving group and the S2B sulfhydryl ready to reseal the binding site, returning the enzyme to the E_1 state. Alternatively, further productive reduction and protonation leads to the crucial E_4 state, where a second bridging hydride is formed. Guided by reasonable coordination geometries, we suggest that this occurs again between Fe2 and Fe6, ideally orienting both hydrides for subsequent

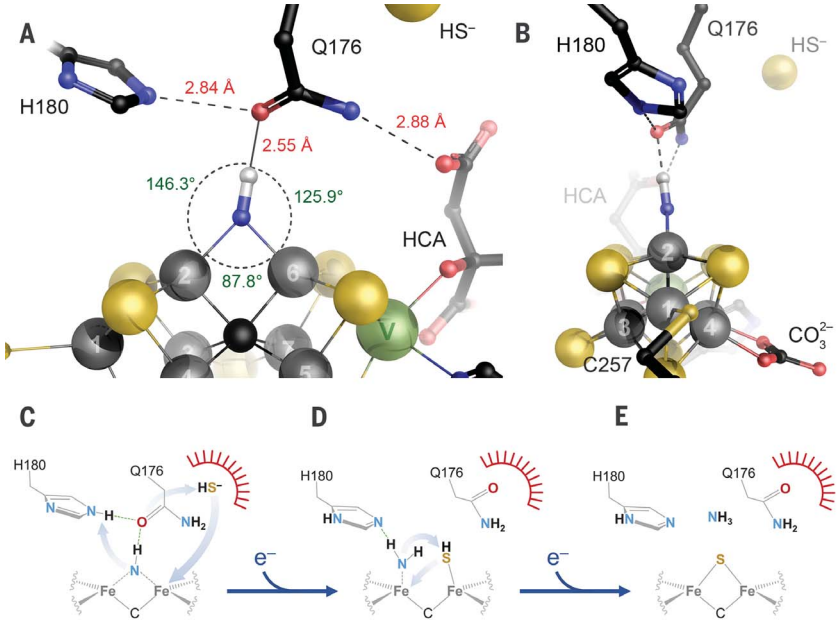

Fig. 3. Intermediate E_6 and the concluding steps of the nitrogenase reaction cycle. (**A**) Bond distances and angles in the structure of the E_6 intermediate, with implicit protonation of the ligand. (**B**) Side view of (A), highlighting the trigonal planar geometry of the nitrogen ligand. (**C**) Schematic representation of the E_6 state with the holding site for HS^- and implicit protonation. Blue arrows indicate rearrangements upon reduction. The red arc indicates the holding pocket for S2B. (**D**) Upon reduction of one Fe site in E_7, the electron can be transferred to the bound ligand, leading to a second protonation, possibly from H180. The NH_2 ligand becomes monodentate, and nucleophilic HS^- rebinds to Fe6, causing Q176 to reorient to its resting-state position. (**E**) After the final reduction, N obtains a further proton, possibly from S2B, and dissociates as product ammonia, and S2B regains the μ-bridging position of the resting state E_0. Alternatively, steps (D) and (E) may occur in a concerted fashion only after the second electron is transferred.

reductive elimination of H_2, which leaves the cofactor in an activated, two-electron-reduced state able to bind N_2 (Fig. 4A). The antiferromagnetic coupling of Fe2 and Fe6 hereby determines that the residual electrons reside on different Fe centers rather than on a single, superreduced site (fig. S11). In its inward-facing conformation, the amide Oε1 atom of Q176 may stabilize the bridging hydrides, but upon elimination of H_2, it readily makes room for an incoming N_2 molecule that undergoes a rapid two-electron reduction from both iron sites, leading to a bridging ligation, similar to the CO complex observed for MoFe protein (*25*). A fundamental difference between the ligands is that the oxygen atom of CO can exclusively serve as an H-bond acceptor, as it does for histidine (fig. S6), but cannot interact with Oε1 of the glutamine, preventing the conformational flip and keeping the holding site inaccessible for S2B. An N_2 molecule reduced by two electrons, however, would be twofold-protonated on the distal nitrogen (Fig. 4B), allowing it to donate hydrogen bonds to both active site residues to drive the reaction forward. In this state, the proximal nitrogen is once more found in an electron-deficient nitrene-like configuration that may be stabilized by electron transfer from the cluster, as described for E_6. All three conformations of the E_4 state (E_4-H2, diferrous E_4*, and E_4-N2H2; Fig. 4C) should readily interconvert, in line with the observed reversibility of N_2 binding and the known ability of nitrogenase to generate HD from D_2 (*29*, *39*).

Further along the reaction pathway, the enzyme is now committed to the complete reduction of the bound intermediate. The reduction step that follows creates the odd-electron, diamagnetic E_5 intermediate, with reduction occurring on the cluster. N–N bond cleavage only occurs upon the transition from E_5 to E_6, when the next electron cannot be accommodated in the cluster itself. Possibly via transient formation of a surface hydride, a two-electron transfer to both nitrogen atoms releases the distal N as NH_3 but retains the proximal one as NH, as observed in the crystal structure. Our proposed reaction scheme thus starts after the distal pathway of N_2 reduction (*40*), but it no longer fits this model at the important transition of E_5 to E_6, where the N–N bond is eventually cleaved. An alternative pathway of N_2 reduction may be straightforwardly envisioned by starting from the open and reduced E4* state and binding N_2 in a side-on (μ-η^2:η^2) mode at Fe2 and Fe6. This would directly lead to the intermediate diazene, but subsequently to hydrazine bound at E_6, which is not congruent with our structural data (fig. S7D). On the other hand, this binding mode might apply to another important substrate, acetylene (C_2H_2). In contrast to N_2 and CO, this compound

Corrected 28 September 2020. See full text.

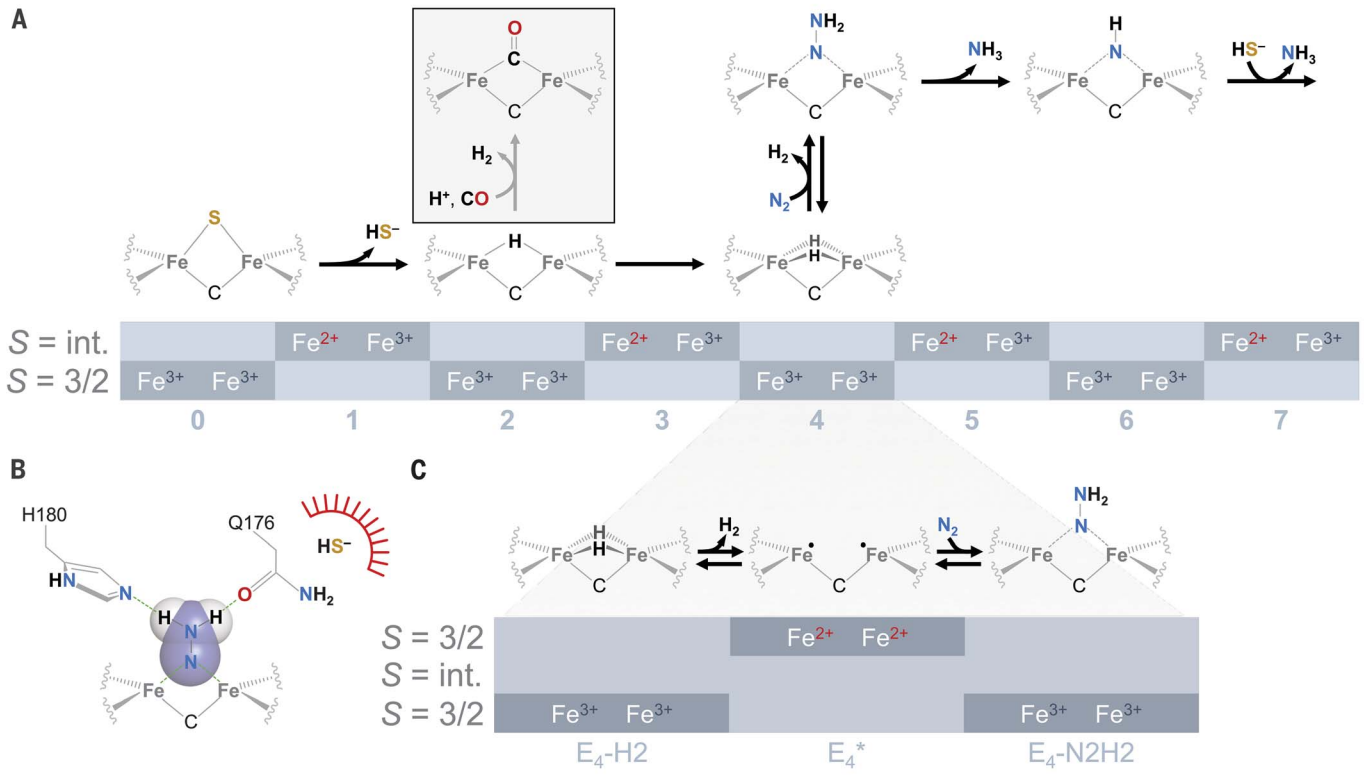

Fig. 4. Stepwise reduction of N_2 on nitrogenase cofactor and CO inhibition. (**A**) Nitrogenase cofactors alternate between an oxidized (M^N, $S = 3/2$) and a one-electron-reduced (M^{1-}, integer spin) state, so that the reduction of N_2 may be described in two-electron steps. From the resting state E_0, reduction to E_2 leads to the formation of the first hydride. If this is lost owing to protonation, the state is susceptible to CO inhibition and consequently may have already eliminated HS^-. The critical E_4 state holds two hydrides and binds N_2 upon reductive elimination of H_2. After two further reduction steps to E_6, the first NH_3 is released, and the proximal nitrogen undergoes the first change of oxidation state. Horizontal arrows represent two-electron transfer events. (**B**) An analogous arrangement of H180 and Q176 can also accommodate bound N_2 after double protonation in the E_4 state, but without forming a hydrogen bond between the amino acid residues, requiring a hypothetical rearrangement of Q176. (**C**) As the key intermediate, the E_4 state is generated by formation of two bridging hydrides (E_4-H2). Reductive elimination of H_2 leaves Fe2 and Fe6 in a highly reactive, doubly reduced state (E_4*) that can bind N_2 and immediately transfer two electrons (E_4-N2H2). These steps are reversible, explaining HD formation in the presence of D_2.

is reduced by two electrons to ethylene (C_2H_4) and to a lesser degree to ethane (C_2H_6) by V nitrogenase (*41*). Cleavage of the C–C bond does not occur, and although we take this as an indication that the μ–η^2:η^2 binding of N_2 is not part of the productive ammonium production reaction, it may well play a role in the reported formation of hydrazine by V nitrogenase (*42*), as well as in the trapping of hydrazine in a variant of MoFe protein (*43*).

Although this outline of a step-by-step mechanism for nitrogenase remains hypothetical, it reconciles existing biochemical data with new structural information, based on the direct observation of an accessible binding site with a bound catalytic intermediate of N_2 reduction by nitrogenase. Our findings are consistent with a bridging hydride replacing sulfide S2B at E_2. Possibly only after H_2 loss through protonation, the open binding site at Fe2 and Fe6 of the cofactor becomes the binding site for less critical substrates such as C_2H_2 and CO, whereas N_2 binding requires E_3 or E_4. These concepts open new avenues for biochemical and theoretical investigations and can be used for a reassessment of the large amount of available spectroscopic and functional data. They furthermore provide a sound basis for the generation and characterization of other reaction intermediates, in particular the mechanistically crucial N_2-bound E_4 state, to complement the kinetic scheme with a detailed structural and electronic analysis.

REFERENCES AND NOTES

1. V. Smil, *Sci. Am.* **277**, 76–81 (1997).
2. D. Fowler, J. A. Pyle, J. A. Raven, M. A. Sutton, *Philos. Trans. R. Soc. London B Biol. Sci.* **368**, 20130165 (2013).
3. Y. L. Hu, M. W. Ribbe, in *Nitrogen Fixation: Methods and Protocols*, M. W. Ribbe, Ed. (Springer, 2011), pp. 3–7.
4. D. C. Rees *et al.*, *Philos. Trans. A Math. Phys. Eng. Sci.* **363**, 971–984, discussion 1035–1040 (2005).
5. O. Einsle *et al.*, *Science* **297**, 1696–1700 (2002).
6. T. Spatzal *et al.*, *Science* **334**, 940 (2011).
7. R. R. Eady, *Chem. Rev.* **96**, 3013–3030 (1996).
8. K. M. Lancaster *et al.*, *Science* **334**, 974–977 (2011).
9. R. Björnsson *et al.*, *Chem. Sci. (Camb.)* **5**, 3096–3103 (2014).
10. O. Einsle, *J. Biol. Inorg. Chem.* **19**, 737–745 (2014).
11. D. Sippel, O. Einsle, *Nat. Chem. Biol.* **13**, 956–960 (2017).
12. J. L. Crossland, D. R. Tyler, *Coord. Chem. Rev.* **254**, 1883–1894 (2010).
13. C. C. Lee, Y. Hu, M. W. Ribbe, *Science* **329**, 642 (2010).
14. W. A. Bulen, J. R. LeComte, *Proc. Natl. Acad. Sci. U.S.A.* **56**, 979–986 (1966).
15. F. B. Simpson, R. H. Burris, *Science* **224**, 1095–1097 (1984).
16. R. N. F. Thorneley, D. J. Lowe, in *Molybdenum Enzymes*, T. G. Spiro, Ed. (Wiley-Interscience, 1985), vol. 1, pp. 221–284.
17. J. Liang, R. H. Burris, *Proc. Natl. Acad. Sci. U.S.A.* **85**, 9446–9450 (1988).
18. B. K. Burgess, S. Wherland, W. E. Newton, E. I. Stiefel, *Biochemistry* **20**, 5140–5146 (1981).
19. R. Y. Igarashi *et al.*, *J. Am. Chem. Soc.* **127**, 6231–6241 (2005).
20. L. C. Seefeldt, B. M. Hoffman, D. R. Dean, *Annu. Rev. Biochem.* **78**, 701–722 (2009).
21. P. E. Doan *et al.*, *J. Am. Chem. Soc.* **133**, 17329–17340 (2011).
22. D. Lukoyanov, B. M. Barney, D. R. Dean, L. C. Seefeldt, B. M. Hoffman, *Proc. Natl. Acad. Sci. U.S.A.* **104**, 1451–1455 (2007).
23. D. Lukoyanov *et al.*, *J. Am. Chem. Soc.* **133**, 11655–11664 (2011).
24. B. M. Hoffman, D. Lukoyanov, Z. Y. Yang, D. R. Dean, L. C. Seefeldt, *Chem. Rev.* **114**, 4041–4062 (2014).
25. T. Spatzal, K. A. Perez, O. Einsle, J. B. Howard, D. C. Rees, *Science* **345**, 1620–1623 (2014).
26. D. J. Lowe, K. Fisher, R. N. F. Thorneley, *Biochem. J.* **272**, 621–625 (1990).
27. R. Y. Igarashi *et al.*, *J. Biol. Chem.* **279**, 34770–34775 (2004).
28. K. Fisher, M. J. Dilworth, C. H. Kim, W. E. Newton, *Biochemistry* **39**, 2970–2979 (2000).
29. K. Fisher, M. J. Dilworth, W. E. Newton, *Biochemistry* **39**, 15570–15577 (2000).

30. R. Ménard, A. C. Storer, *Biol. Chem. Hoppe Seyler* **373**, 393–400 (1992).
31. S. D. Brown, M. P. Mehn, J. C. Peters, *J. Am. Chem. Soc.* **127**, 13146–13147 (2005).
32. D. Lukoyanov *et al*., *Proc. Natl. Acad. Sci. U.S.A.* **109**, 5583–5587 (2012).
33. J. B. Varley, Y. Wang, K. Chan, F. Studt, J. K. Nørskov, *Phys. Chem. Chem. Phys.* **17**, 29541–29547 (2015).
34. Z. Y. Yang *et al*., *Biochemistry* **55**, 3625–3635 (2016).
35. D. Lukoyanov *et al*., *J. Am. Chem. Soc.* **138**, 1320–1327 (2016).
36. B. M. Hoffman, D. Lukoyanov, D. R. Dean, L. C. Seefeldt, *Acc. Chem. Res.* **46**, 587–595 (2013).
37. T. Spatzal *et al*., *Nat. Commun.* **7**, 10902 (2016).
38. D. J. Lowe, R. N. F. Thorneley, *Biochem. J.* **224**, 895–901 (1984).
39. B. K. Burgess, D. J. Lowe, *Chem. Rev.* **96**, 2983–3012 (1996).
40. I. Djurdjevic, O. Einsle, L. Decamps, *Chem. Asian J.* **12**, 1447–1455 (2017).
41. P. M. C. Benton, J. Christiansen, D. R. Dean, L. C. Seefeldt, *J. Am. Chem. Soc.* **123**, 1822–1827 (2001).
42. M. J. Dilworth, R. R. Eady, *Biochem. J.* **277**, 465–468 (1991).
43. B. M. Barney *et al*., *Biochemistry* **44**, 8030–8037 (2005).

ACKNOWLEDGMENTS

We thank F. Meyer and R. Björnsson for helpful discussions; the beamline staff at the Swiss Light Source, Villigen, Switzerland, for excellent assistance with data collection; and B. Prasser for EPR measurements. **Funding**: This work was supported by the European Research Council (grant no. 310656), the Deutsche Forschungsgemeinschaft (RTG 1976 and PP 1927), and the BIOSS Centre for Biological Signalling Studies at Albert-Ludwigs-Universität Freiburg. **Author contributions**: D.S., M.R., J.N., C.T., J.G., K.G., I.D., and L.D. performed the experiments; D.S., S.L.A.A., and O.E. designed the experiments and processed data; D.S. and O.E. built and refined the structural model; and O.E. wrote the manuscript.

Competing interests: The authors declare no conflicts of interest. **Data and materials availability**: Raw data and additional material are available from the corresponding author upon request. The structural model and structure factors have been deposited in the Protein Data Bank with accession code 6FEA. Anomalous dispersion data for the VFe protein turnover state are available at https://zenodo.org/record/4024212#.X2ylppNKhAm.

SUPPLEMENTARY MATERIALS

www.sciencemag.org/content/359/6383/1484/suppl/DC1
Materials and Methods
Figs. S1 to S11
Table S1
References (*44*–*57*)

20 October 2017; accepted 31 January 2018
10.1126/science.aar2765